Global mapping of changes in landscapes and coverages of vegetation types from the ESA land cover 1992-2015 time series

Jakub Nowosad, Tomasz F. Stepinski*, Pawel Netzel

Space Informatics Lab, Department of Geography and GIS, University of Cincinnati, Cincinnati, USA, OH 45221-0131, USA

Abstract

Monitoring global land cover changes is important because of concerns about their impact on environment and climate. To enable such monitoring we present a global, GIS-based database of land cover changes during the 1992–2015 period. The database uses the new ESA global time series of land cover maps at 300m resolution (CCI-LC). The spatial unit of the database is a local landscape – a 9km × 9km tile consisting of 900 CCI-LC pixels. The entire landmass is tessellated into such tiles and a pattern-based similarity between a pair of 1992 and 2015 landscape mosaics in each tile is calculated to identify a zone of significant change. Such zone was found to constitute the 22% of the landmass. For each tile in the change zone, the following attributes were calculated: transition matrix between CCI-LC categories, a set of change trajectories, and a composition of plant functional types (PFTs). The result is a comprehensive but relatively compact SQL-searchable database to be used for analyzing land cover transitions, global mapping of change trajectories, and tracking changes to global distributions of PFTs. Globally dominant CCI-LC transitions during the 1992-2015 period were forest → agriculture (19%) and agriculture → forest (10%). A global map of change trajectories provides a visualization of the spatial distribution of all major changes and serves as a guide to a more focused use of the database. The vegetation type that experienced the largest net loss was the trees at -559,124 km^2 globally. We concluded that using our database is well-suited for a fairly accurate estimation of the global forest area and a depiction of a geographical distribution of forest losses/gains, but, in comparison with estimates stemming from a forest-dedicated change detection method using high resolution images, it provides a low estimation of forest loss and a high estimation of forest gain. For other vegetation types estimations of losses and gains are expected to be more accurate due to more homogeneous definitions of non-forested CCI-LC categories.

Keywords:
Land cover transition, ESA CCI-LC time series, PFT map, forest change

1. Introduction

Land-cover change is a pervasive phenomenon caused by changing climate, and, in recent decades, by the rapid population growth and accelerated industrialization. As a part of a positive feedback loop, land cover changes in turn directly impact climate change and environmental conditions (Grimm et al., 2008; Jones et al., 2008; Mahmood et al., 2014), and have a close relationship to population migration and economic conditions (DeFries, 2013). Thus, the assessment of land-cover changes is of prime importance for the effective planning and management of resources. It provides necessary information for making decisions on a trade-off between development and conservation (Vitousek et al., 1997; DeFries et al., 2004). Multi-temporal remote sensing is the only cost-effective means for assessment of land-cover change. Fortunately, increasing availability of global coverage, multi-temporal, high resolution images makes the assessment of the land cover change possible even on the global scale.

Because of its importance, there is a rich literature on different approaches to detecting and assessing land-cover change from remotely sensed images. These approaches are summarized in several reviews (Coppin et al., 2004; Radke et al., 2005; Warner et al., 2009; Hussain et al., 2013; Lu et al., 2014; Tewkesbury et al.,

*Corresponding author
Email addresses: nowosad.jakub@gmail.com (Jakub Nowosad), stepintz@uc.edu (Tomasz F. Stepinski), pawel@netzel.pl (Pawel Netzel)

2015). From multiple conceptual and technical components which constitute a change detection method we draw attention to three: the unit of analysis (for example, a pixel, a tile, a polygon), the comparison method (for example, a direct spectral comparison or a post-classification comparison) and the change type (for example, "from-to" change trajectories or specific change types). In general, the most frequently used method uses a pixel as the unit of analysis and a post-classification change detection (Tewkesbury et al., 2015). However, on the global scale, the change assessments have focused on the detection of a specific change, namely deforestation (Hansen et al., 2010, 2013; Kim et al., 2014), rather than on the comprehensive, "from-to" change.

To the best of our knowledge, no single map showing all "from-to" changes in land cover categories has been published. This is because such assessment requires the production of temporally consistent global thematic maps of land cover at multiple time periods. Until recently such maps were not available. The MODIS Collection 5 land cover product (MCD12Q1) (Friedl et al., 2010) provides annually updated global land cover maps since 2001 at 500 m resolution, but it is not constructed to be temporally consistent (Cai et al., 2014), and, consequently, is not well-suited for change assessment. Wang et al. (2015) described a process of producing global maps of land cover for 2001 and 2010 with spatio-temporal consistency improved over MCD12Q1, but this dataset is not available in the public domain. Recently, the European Space Agency (ESA) Climate Change Initiative (CCI) program released (http://maps.elie.ucl.ac.be/CCI) a temporally consistent time series of global land cover maps at 300 m resolution spanning a 23-year period, from 1992 to 2015. This dataset is thereafter referred to as CCI-LC. The temporal consistency of the series was a primary objective of the project and was achieved by decoupling land cover mapping and change detection (ESA, 2017). Thus the CCI-LC dataset could be used for the comprehensive, "from-to" global assessment of land cover change.

The major goal of the project described in this paper is to develop a Geographical Information System (GIS) database which facilitates analysis and visualization of comprehensive land cover change on a global scale over almost a quarter of a century (1992 to 2015). Our design criteria for the database are as follows. (A) It is made especially for the global-scale change analysis. (B) The database has a small enough size to work well on a majority of computers and yet it incorporates all pertinent information contained in 1992 and 2015 CCI-LC maps. (C) It contains plant functional types (PFTs) distribution for mapping changes of cover for different vegetation types. (D) It supports SQL search. (E) It provides a compelling visualization of land cover change in a single thematic map of change trajectories.

To achieve these design criteria we decouple the analysis into a change detection and change characterization phases. For the change detection, we use the method first described by Netzel and Stepinski (2015). This method uses a tile as the unit of analysis. A tile is a square tract of land consisting of a large number of pixels (for this study a size of 900 pixels is selected). The pattern of land cover categories within a tile form a local landscape mosaic. We calculate a dissimilarity value (a single number) between tile's landscape mosaics in 1992 and 2015 as an assessment of landscape change.

Detecting change at the level of a 9km $\times$ 9km tile instead of 300m $\times$ 300m pixel has several advantages for a change analysis on the global-scale. (1) It smooths possible errors stemming from incorrect category assignments at individual pixels. (2) Because tiles are compared using rotationally and translationally invariant dissimilarity measure, a mere re-arrangement of category assignments without changing an overall composition and configuration of landscape mosaic is not going to be detected as a change. This avoids a possible confusion found, for example, in the studies of global, pixel-based forest cover change (Hansen et al., 2013; Kim et al., 2014) where geographically relevant areas contain pixels labeled as forest loss as well as those labeled as forest gain. (3) Using tiles instead of pixels reduces the number of units of analysis by orders of magnitudes making possible construction of the relatively compact spatial database. Each tile carries multiple attributes describing in details the change in landscape mosaic within the tile. The database is SQL-searchable making possible finding a global geographical distribution of regions that underwent a type of change as specified by an analyst. (4) Finally, a larger spatial scale of tiles results in a more compelling visualization of change assessment.

For change characterization phase we first divide the tiles into “changed” and “unchanged” using an empirically determined dissimilarity value as a threshold. Note that unchanged tiles are not necessarily identical in 1992 and 2015, instead, the change in their mosaic is negligible at the scale of the tile. Only changed tiles are subject to change characterization. For each pixel in a changed tile, we calculate a transition between land cover categories in 1992 and 2015. A histogram of pixels' transitions within a tile characterizes a change in this tile and is saved to the database as attributes of the tile. Transitions are further classified into a smaller

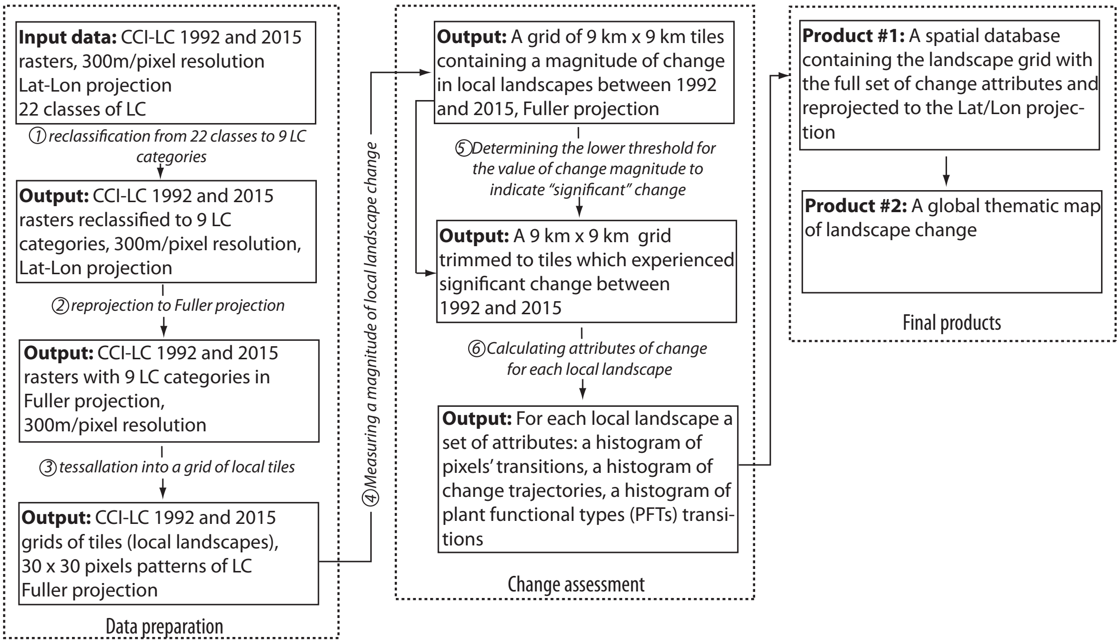

Figure 1: Diagram outlining consecutive computational steps to obtain a landscape change database. Numbers in circles label calculation steps described in the main text.

number of generalized "change trajectories" and the histogram of change trajectories is also saved as attributes of the tile. Change trajectories are used to produce a thematic map of change, an encapsulation of geographical distribution of all land cover changes across the entire landmass. Finally, we also translate 1992 and 2015 categories within a tile to PFTs using a conversion table (Poulter et al., 2015) and save PFTs transitions as tile's attributes. PFTs are used to assess cumulative change of a single, specific vegetation type, for example, the trees.

2. Data and methods

In this section, we describe the CCI-LC dataset, a change detection method, and change characterization method. Fig. 1 shows a diagram outlining consecutive computational steps taken to produce a landscape change database and the global thematic map of change.

2.1. Data

We use the CCI-LC 1992 and 2015 global maps of land cover as an input to the landscape change analysis. We have chosen to assess change over a maximum time lag available in the CCI-LC data. Details about the CCI-LC dataset can be found in the Land Cover CCI Product User Guide V.2 (ESA, 2017). The CCI-LC maps are in the form of 64,800 $\times$ 129,600 Lat/Lon raster, thus its spatial resolution is 10 arc-sec or ~300 m at the equator. Each pixel is assigned one of 22 land cover classes. However, only 9 broader land categories were considered for the change detection (ESA, 2017). Thus, we first have reclassified (step 1) the two maps from 22 classes to 9 categories (see Fig. 2 for the legend of the 9 broader categories, and see the CCI-LC User Guide for correspondence between classes and categories). The CCI-LC map in the Lat/Lon projection cannot be globally divided into tiles having all the same shapes and physical sizes. Therefore we reproject (step 2) the 1992 and 2015 maps into the Fuller projection (Gray, 1995) with 300 m resolution to keep distortions of tiles' real shapes and sizes below 2%. Fuller-projected maps are tessellated (step 3) into non-overlapping square tiles of the size 30$\times$30 pixels (9 km $\times$ 9 km). The size of a tile is a free parameter which determines the scale on which the change of landscape is assessed. Given the resolution of CCI-LC our choice of tile's size is small enough to provide a high resolution on the global scale but large enough for tiles to encompass meaningful landscapes.

2.2. Change detection

We calculate (step 4) a dissimilarity value between 1992 mosaic and 2015 mosaic in each tile. Quantita-

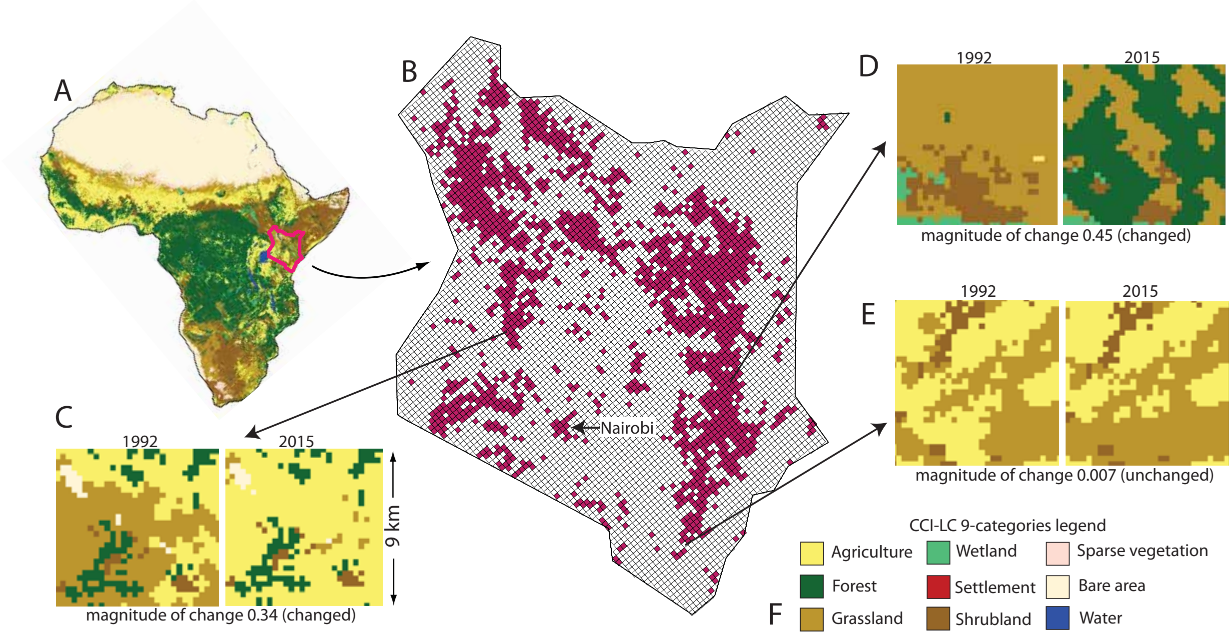

Figure 2: Methodology of change detection shown using the country of Kenya as an example. (A) 2015 CCI-LC map of Africa, the red outline indicates the location of Kenya. (B). The area of Kenya divided into a grid of 9 km × 9 km tiles, red tiles indicate where landscape mosaic has changed during the 1992-2015 period. (C)–(D) Examples of changed tiles. (E) An example of an unchanged tile. (F) Legend of 9-categories CCI-LC map.

tive assessment of dissimilarity between two landscape mosaics requires a mathematical representation of the mosaic and a definition of a dissimilarity function.

A mosaic (pattern of land cover categories) in a tile is mathematically described by a normalized histogram (the sum of all its bins equals to 1) of land cover category co-occurrence pattern features (Barnsley and Barr, 1996; Chang and Krumm, 1999). Briefly, pattern features are the pairs of land cover categories assigned to two neighboring pixels. Histogram counts and bins the features from eight co-occurrence matrices calculated for eight different displacement vectors along the eight principal directions (see Niesterowicz et al. (2016) for an illustrative example). The result is a histogram with $(N^2 + N)/2$ bins, where N is the number of land cover categories; for 9-categories CCI-LC the histogram has 45 bins. Such histogram describes (indirectly but effectively, see Niesterowicz and Stepinski (2016)) composition as well as the spatial configuration of land cover categories within a tile and thus the landscape mosaic within a tile.

We use the Jensen-Shannon Divergence (JSD) (Lin, 1991) as a measure of dissimilarity between two mosaics (one for 1992 and another for 2015 within the same tile) represented by corresponding normalized histograms M_{1992} and M_{2015}. The JSD expresses the informational distance between the two histograms as a deviation between Shannon's entropy of the conjugate of the two histograms $(M_{1992} + M_{2015})/2$ and the mean entropy of individual histograms M_{1992} and M_{2015}. The value of JSD, denoted by $d(M_{1992}, M_{2015})$, is given by the following formula:

$$d(M_{1992}, M_{2015}) = H\left(\frac{M_{1992} + M_{2015}}{2}\right) - \frac{H(M_{1992}) + H(M_{2015})}{2} \tag{1}$$

where $H(M)$ indicates a value of the Shannon's entropy of the histogram M:

$$H(M) = -\sum_{i=1}^{|N|} m_i \log_2 m_i. \tag{2}$$

where m_i is the value of $i th$ bin in the histogram M and $|N|$ is the number of bins (the same for both histograms). For normalized histograms, the JSD dissimilarity always takes values from 0 to 1 with the value of 0 indicating that two mosaics have identical histograms, and

Table 1: Reclassification of land cover transitions into land cover trajectories

from 1992 \ to 2015	Agriculture	Forest	Grass	Wetland	Settlement	Shrub	Sparse	Bare	Water
Agriculture	**Stable**	Forest ↑	Crop ↓	Wetland ↑	Urban ↑	Shrub ↑	Crop ↓	Crop ↓	Water ↑
Forest	Forest ↑	**Stable**	Forest ↓	Forest ↓	Urban ↑	Forest ↓	Forest ↓	Forest ↓	Water ↑
Grass	Crop ↑	Forest ↑	**Stable**	Wetland ↑	Urban ↑	Shrub ↑	Grass ↓	Grass ↓	Water ↑
Wetland	Wetland ↓	Forest ↑	Wetland ↓	**Stable**	Urban ↑	Wetland ↓	Wetland ↓	Wetland ↓	Water ↑
Settlement	*Urban* ↓	*Urban* ↓	*Urban* ↓	*Urban* ↓	**Stable**	*Urban* ↓	*Urban* ↓	*Urban* ↓	*Urban* ↓
Shrub	Crop ↑	Forest ↑	Grass ↑	Wetland ↑	Urban ↑	**Stable**	Shrub ↓	Shrub ↓	Water ↑
Sparse	Crop ↑	Forest ↑	Grass ↑	Wetland ↑	Urban ↑	Shrub ↑	**Stable**	**Stable**	Water ↑
Bare	Crop ↑	Forest ↑	Grass ↑	Wetland ↑	Urban ↑	Shrub ↑	**Stable**	**Stable**	Water ↑
Water	Water ↓	Water ↓	Water ↓	Water ↓	Urban ↑	Water ↓	Water ↓	Water ↓	**Stable**

↑ indicates gain, ↓ indicates loss, slanted font indicates non-occurring trajectories

the value of 1 indicating maximum dissimilarity (none of the land cover categories found in one mosaic can be found in the other). The dissimilarity value is used as a quantitative assessment of the magnitude of change, the larger the dissimilarity the bigger the change.

To divide the tiles into "changed" and "unchanged" we determined (step 5) the value of dissimilarity threshold d_{th}, Tiles with $d(M_{1992}, M_{2015}) > d_{th}$ are considered as changed and tiles with $d(M_{1992}, M_{2015}) \leq d_{th}$ are considered as unchanged. For threshold determination we have selected a random, stratified sample of 1000 tiles. We labeled these tiles either as changed or unchanged based on visual inspection of tiles' mosaics in 1992 and 2015. Applying a decision tree algorithm to a dataset consisting of $(d(M_{1992}, M_{2015}), \text{label})_\text{i}$, $i = 1, \ldots, 1000$ yields $d_{th} = 0.012$.

Fig. 2 illustrates our concept of change detection using the country of Kenya as an example. Fig. 2B shows the outline of Kenya tessellated into 9 km × 9 km tiles. Examples of landscape mosaics in 1992 and 2015 in three tiles are shown in panels C, D, and E of Fig. 2. Two tiles, C and D, labeled as changed, clearly exhibit a change in landscape mosaic, while the tile E, labeled as unchanged, shows no change in it mosaic even so a small number of pixels had transitioned. Red-colored tiles in Fig. 2B indicate areas where landscape mosaic has changed between 1992 and 2015. Note that landscape mosaics in the majority of Kenya's territory had not changed between 1992 and 2015. Globally, of 1,640,016 tiles, only 363,137 (22%) had changed their landscape mosaics during this period under our definition.

2.3. Change characterization

Only changed tiles are subject to change characterization. Thus, we concentrate on the most dynamic portion of the terrestrial landmass where landscape mosaic had significantly changed during the 1992-2015 period. The remaining portion of the landmass also experienced change but on the much smaller spatial scale leaving 9 km-scale landscapes unchanged. Change characterization aims at an explicit description of the change. Descriptors of change are calculated and saved as tiles' attributes. Geographical locations of tiles and their attribute information constitute a spatial database of change in the portion of the terrestrial landmass with the strongest landscape dynamics.

Bins of a histogram of "from-to" transitions aggregated from 900 pixels within a tile make up the first set of tile's attributes. With 9 land categories there are potentially 72 types of transitions, but since no pixel with the "settlement" category changed to another category during the 1992-2015 period (see section 3) there are actually only 64 types of transitions. For each tile we save a histogram with 65 bins (most of them equal to 0), the additional bin is a share of 900 pixels that did not change their category. The bins are normalized to shares so they all sum to 1. These attributes provide the most detailed and direct information on change within a tile. Analysts may use these attributes to search the landmass for geographic locations where specific transitions occurred at a specified range of intensities.

However, a global map of 64 "from-to" transitions would be too busy to be informative. Therefore, we generalize 64 transitions into 13 "change trajectories": cropland gain, cropland loss, forest gain, forest loss, grassland gain, grassland loss, shrubland gain, shrubland loss, wetland gain, wetland loss, urban gain, water gain, and water loss. Table 1 shows the reclassification from transitions to trajectories. Note that in this reclassification we don't distinguish between sparse and bare CCI-LC categories. Reduction of the number of change types causes information loss as multiple transitions are

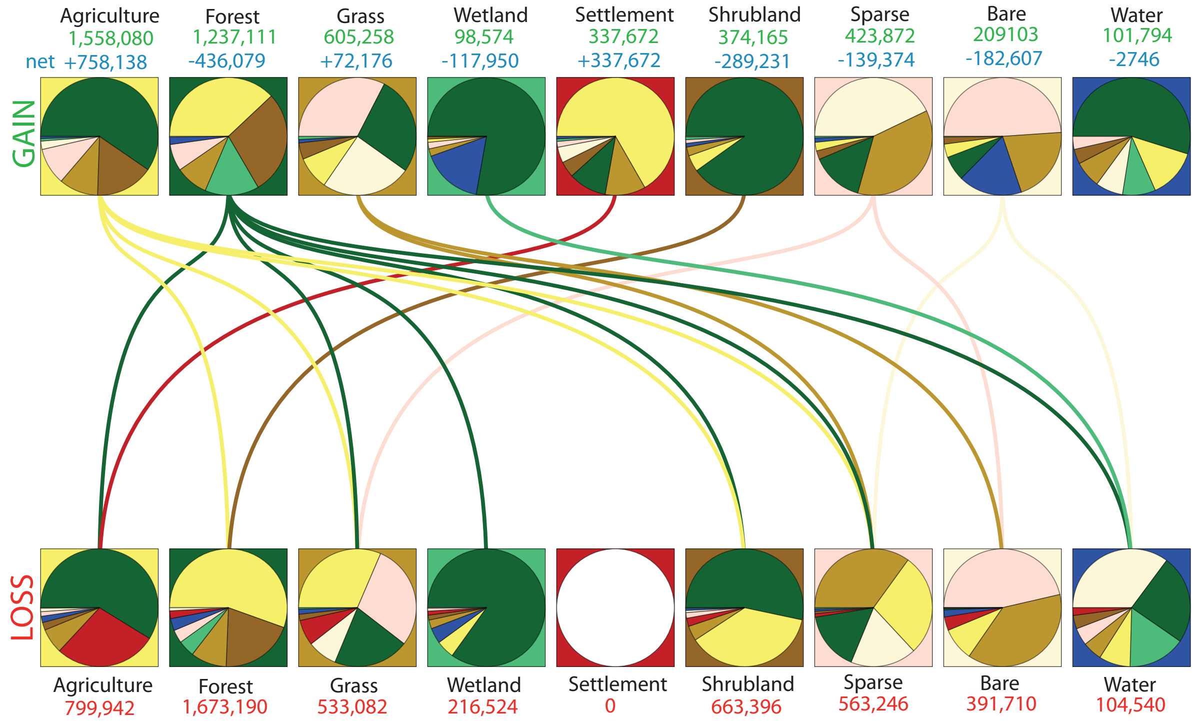

Figure 3: Global summary of major 1992–2015 transitions between the nine CCI-LC categories. See the main text for a detailed description of the diagram. Loss, gain, and net numbers are in km^2. For the legend to CCI-LC categories see Fig.2.

reclassified to a single trajectory. The labels of trajectories reflect our assumed priority. For example, an agriculture → grassland transition is classified as "cropland loss" but it could also be classified as "grass gain."

Bins of a histogram of trajectories aggregated from 900 pixels within a tile make up the second set of tile's attributes. For each tile we save 14 bins, the additional bin is a share of 900 pixels with stable trajectories. The values are normalized to shares so they all sum to 1. These attributes provide generalized (less detailed) information on change within a tile. However, in many cases the generalized change information is sufficient. For 77% of the tiles, a single trajectory completely dominates types of change within a tile (on average 96% of changed pixels in the tile are assigned to a dominant trajectory). For the remaining 23% of tiles on average, 63% of changed pixels are assigned to a dominant trajectory. Thus, a trajectory of change for the entire tile can be inherited from the dominant trajectory of its constituent pixels.

For a global thematic map of landscape change, each tile is assigned a color on the basis of its change trajectory and the percentage of changed pixels. Tiles where this percentage is > 30% are classified as "large change", those where this percentage is between 10% and 30% are classified as "medium change", and those where this percentage is below 10% are classified as "small change." Altogether, the map has 39 categories, each a combination of its trajectory, which describes a type of change, and the magnitude, which indicates a percentage of tile's area that had changed.

The final set of tile's attributes is its plant functional types (PFTs) composition. PFT is a plant classification based on their physical, phylogenetic and phenological characteristics. For studying the global change of natural vegetation, maps of PFTs may be more accurate than maps of land cover classes (B.Bonan et al., 2002; Poulter et al., 2011). We calculate composition of PFTs in each pixel using a cross-walking table (Poulter et al., 2015) between 22 CCI-LC classes and 13 PFTs (broadleaf evergreen tree, broadleave deciduous tree, needleleaf evergreen tree, needleleave deciduous tree, broadleaf evergreen shrub, broadleave deciduous shrub, needleleaf evergreen shrub, needleleave deciduous shrub, natural grass, managed grass, bare soil, water, snow/ice). Aggregation of PFTs compositions from

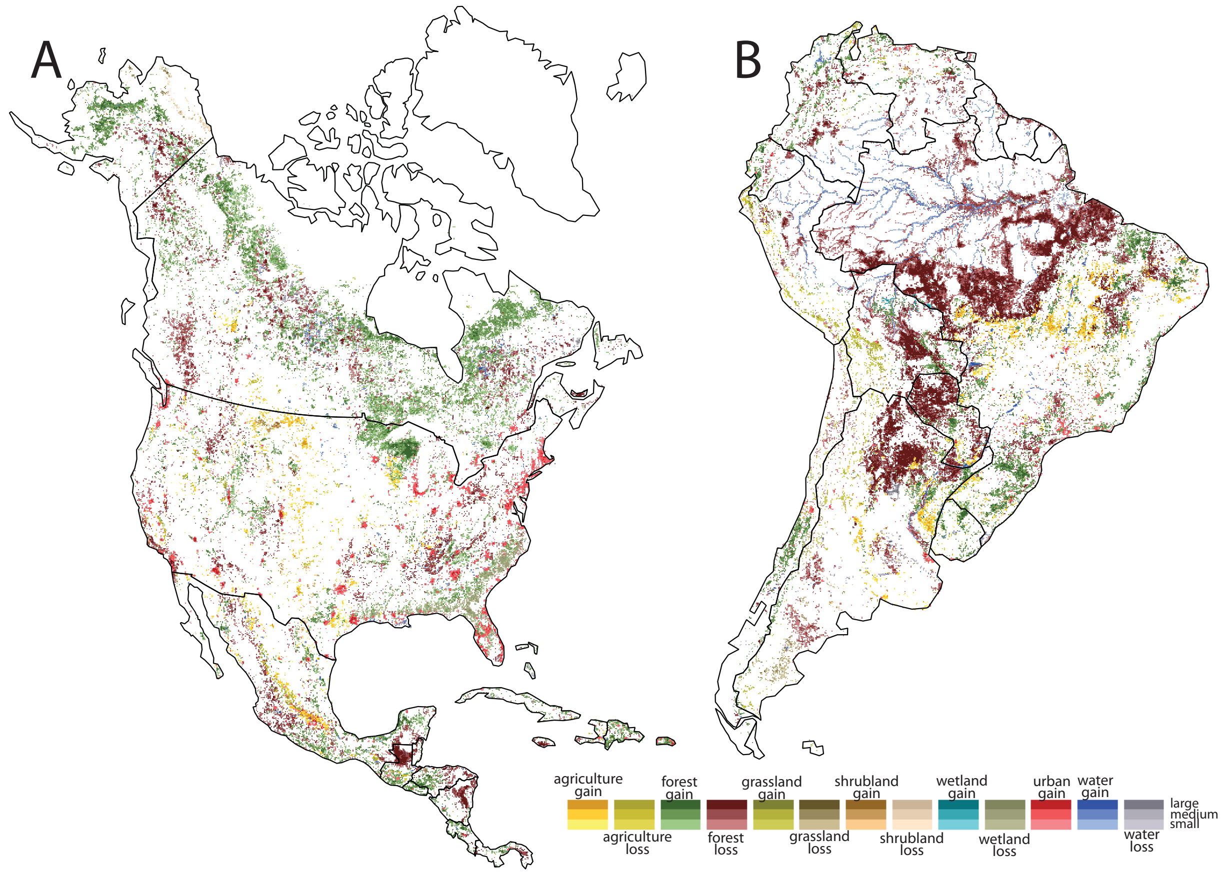

Figure 4: Map of 1992-2015 landscape change trajectories for North America (A) and South America (B). Local landscapes are colored depending on their change trajectories and a percentage of changed area; small < 10%, medium (10% to 30%), and large (> 30%).

900 constituting pixels gives their composition in the entire tile.

3. Results

The major product of this project is the spatial database of 1992–2015 landscape change constructed as described in the previous section. This database is available for download from http://sil.uc.edu. The distributed database is projected back to Lat/Lon coordinates. Here we present the global summary of landscape change using the three sets of database attributes, transitions, trajectories, and PFTs.

3.1. Global summary of transitions

Fig. 3 summarizes information from 1992–2015 transitions between CCI-LC categories. The lower row of pie-diagrams pertains to losses in consecutive land cover categories. The red numbers below pie-diagrams indicate total loss of an area (in km^2) in a given land cover category to other land cover categories. A pie diagram illustrates a percentage breakup of this loss going to other categories. For example, during 1992–2015 period 799,942 km^2 was lost from the agriculture. The pie diagram indicates that most of this loss was to the forest (60%) and the settlement (28%). The upper row of pie-diagrams pertains to global gains in consecutive land cover categories. The green numbers above pie-diagrams indicate the total gain in an area (in km^2) of a given land cover category from other land cover categories. A pie diagram illustrates a percentage breakup of this gain coming from other categories. For example, during 1992–2015 period 1,558,080 km^2 was gained by the agriculture. The pie diagram indicates that most of this gain was from the forest (60%), shrubland (16%), grassland (11%), and sparse (10%). Transitions larger than 10% of category loss are illustrated by lines connecting the loss pie-diagrams with gain pie-

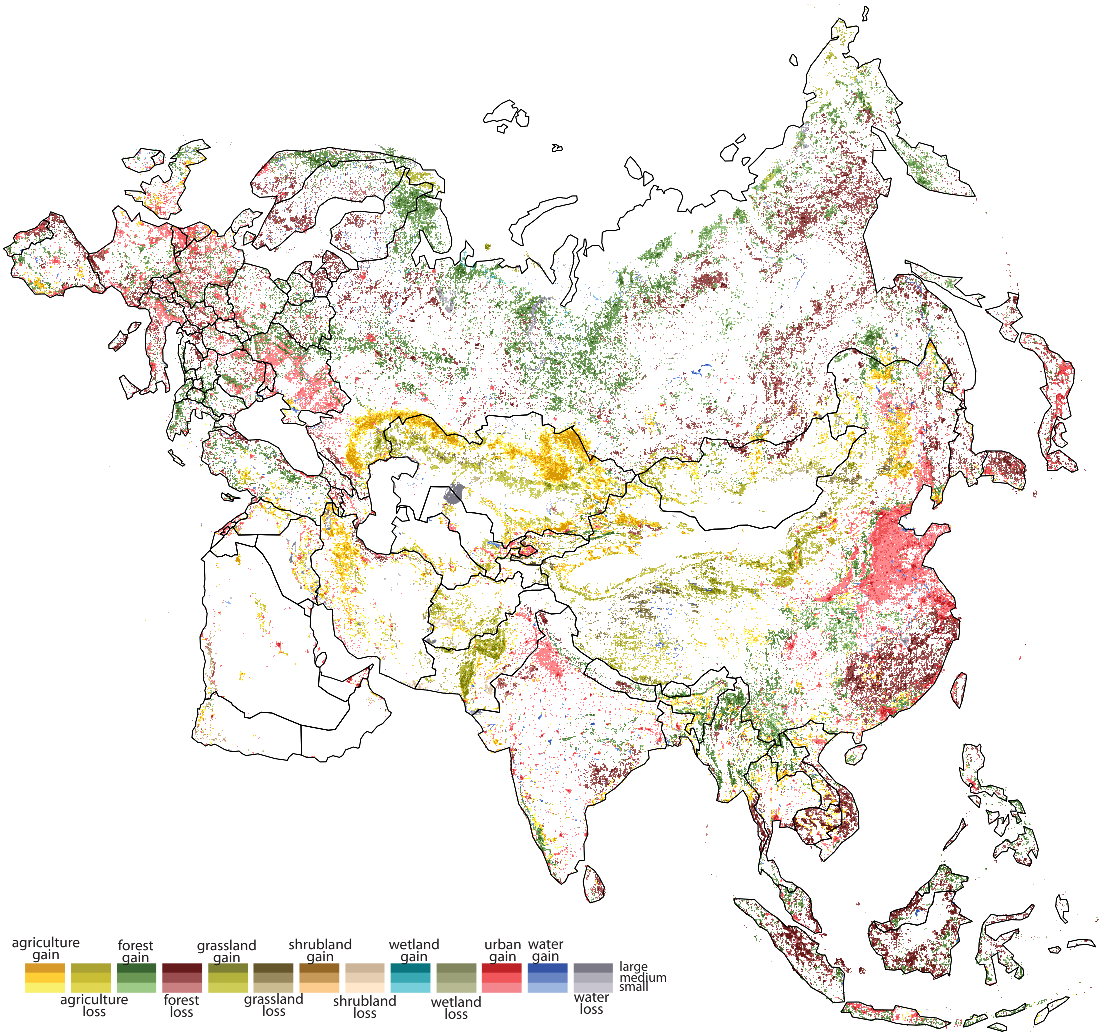

Figure 5: Map of 1992-2015 landscape change trajectories for Eurasia. Local landscapes are colored depending on their change trajectories and a percentage of changed area; small < 10%, medium (10% to 30%), and large (> 30%)

diagrams; colors of the lines indicate the destination and the widths are proportional to the percentage of the loss going to a given destination. The blue numbers indicate the net change in an area (in km^2) of a given land cover category; for example, a net change in an area covered by agriculture was +758,138 km^2.

3.2. Global map of landscape change trajectories

Portions of the global map of change trajectories are shown in Fig.4 (North and South America), Fig.5 (Eurasia), and Fig.6 (Africa and Australia). A single change map for the entire world is given in Supplement 1. The map shows a geographical distribution of different types of landscape change. Recall from section 2.2 that only 22% of local landscapes (tiles) has changed. The fact that this percentage appears to be larger on Figs. 4–6 is due to graphic rendition; the map needs to be zoomed in to reflect the true size of the changed area. It is also important to stress that only a fraction of an area within a changed tile had transitioned. In 62% of changed tiles, less than 10% of the area had changed; these tiles are labeled as "small change" tiles and are drawn on the map in lightest shades. In 26% of changed tiles 10%–30% of the area had changed; these tiles are labeled as "medium change" and are drawn on the map in intermediate shades, In only 12% of changed tiles the area had changed by more than 30%; these tiles are labeled as "large change" and are drawn on the map in darkest

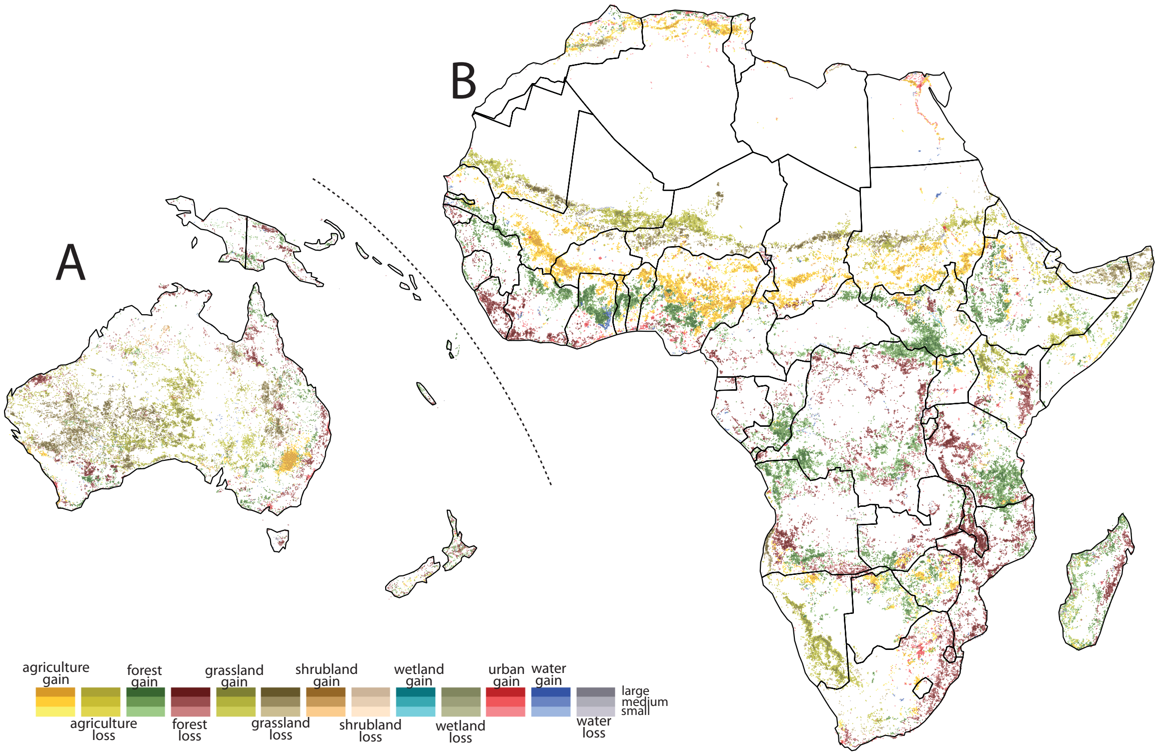

Figure 6: Map of 1992-2015 landscape change trajectories for Australia (A) and Africa (B). Local landscapes are colored depending on their change trajectories and a percentage of changed area; small < 10%, medium (10% to 30%), and large (> 30%)

shades.

The largest areas of intensive forest loss are observed in the tropical regions, but forest loss is also observed elsewhere, in particular in Russia, Scandinavia, Baltic countries, and Canada. The top three transitions responsible for forest loss are forest → agriculture, forest → shrubland, and forest → grassland, together responsible for 84% of the loss. The map also shows significant areas of forest gain, especially in the northern Russia, northern Canada, and in Africa. The top three transitions responsible for forest gain are agriculture → forest, shrubland → forest, and wetland → forest, together responsible for 75% of the gain.

The prominent areas of crop expansion are northern Kazakhstan, southern Russia, northern Iran, Sahel region in Africa, northern Algeria, northeastern China, and New South Wales in Australia. The top three transitions responsible for crop gain are shrubland → agriculture, grassland → agriculture, and sparse vegetation → agriculture, together responsible for 84% of the gain. The growth of urban areas is around preexisting large cities but a more widespread growth around smaller cities is also observed in eastern China, northern India, and parts of Europe. The top three transitions responsible for urban gain are agriculture → urban, grassland → urban, and forest → urban, together responsible for 76% of the gain. Loss of wetlands is a prominent feature along the Atlantic and Gulf coasts of the United States. The top two transitions responsible for wetland loss are wetland → agriculture and wetland → grass, together responsible for 68% of the loss. The most prominent feature of water loss is a disappearance of the Aral Sea, and the most prominent feature of water gain is the Amazonian network, which we speculate is due to either clearing of river banks or increased level of water.

3.3. *Changes to vegetation cover using PFTs*

PFTs attributes in our database allow for calculation of the change in coverage for particular types of vegetation. Table 2 shows the results of such calculations. We have grouped all types of trees and all types of shrubs into "trees" and "shrubs" types. We also have grouped bare soil, water, and snow/ice into one non-vegetated type. This table has two sections, the upper section pertains to "changed" landscapes defined in section 2.2, and the lower section pertains to the entire landmass.

Table 2: Global change in vegetation cover calculated using PFTs

	Trees	Shrub	Nat. Grass	Man. Grass	Non-vegetated
In the area defined as “changed”					
area in 1992	8,496,690	3,917,270	4,916,470	5,772,610	6,315,080
area in 2015	8,034,510	3,722,330	5,003,340	6,421,740	6,236,170
area lost	-1,175,726	-420,803	-391,598	-451,803	-702,012
area gained	+713,552	+225,864	+478,469	+1,100,935	+623,110
net change	**-462,178**	**-194,939**	**+86,871**	**+649,132**	**-78,902**
In the entire landmass area					
area in 1992	33,505,300	16,387,800	19,811,100	21,741,800	52,995,900
area in 2015	32,946,300	16,165,500	19,933,900	22,428,600	52,967,300
area lost	-1,437,286	-507,651	-479,499	-588,094	-819,311
area gained	+878,162	+285,359	+602,368	+1,274,869	+790,683
net change	**-559,124**	**-222,292**	**+122,869**	**+686,775**	**-28,902**

All areas in km^2. Areas in 1992 and 2015 rounded to six significant digits.

For each type, we list areas covered in 1992 and 2015, area lost, area gained, and the net change.

The first observation is that changes to the coverage of plant types occurred, as expected, mainly within the “changed” zone. A percentage of change within this zone, $(\text{area lost + area gained})_{\text{zone}}/(\text{area lost + area gained})_{\text{all}}$, is 82% for trees, 82% for shrub, 80% for natural grass, and 84% for managed grass, and 82% for non-vegetated. A percentage of net change within this zone is 83% for trees, 88% for shrub, 71% for natural grass, and 95% for managed grass. In the non-vegetated part of the landmass, this percentage is 273% indicating that the imbalance between losses and gains of non-vegetated land in the change zone is about three times larger than in the entire landmass.

The second observation is an amount of difference between the net coverage change of vegetation types (the net change line in the upper section of Table 2) and the net change in coverage of corresponding CCI-LC categories (blue line in Fig. 3). The relative difference, $[(\text{net change})_{\text{CCI}} - (\text{net change})_{\text{veg. type}}]/(\text{net change})_{\text{CCI}}$, is 6% between forest and trees, 14% between agriculture and managed grass, 20% between grassland and natural grass, 33% between shrubland and shrub, and 57% between (bare + water) and non-vegetated. Thus, estimating the loss of forest and gain of crops from CCI-LC transitions yields values similar to those estimated on the basis of changes to PFTs coverage, but CCI-LC transitions should not be used to estimate the change in coverage of other vegetation types.

The third observation is about the balance between losses and gains of coverage for different vegetation types. We quantify such balance by calculating a ratio (net change)/(area lost + area gained) using the data in the lower section of Table 2. This ratio is 0.24 for trees, 0.28 from shrub, 0.11 for natural grass, 0.37 for managed grass, and 0.02 for non-vegetated. Thus changes to non-vegetated parts of the landmass are highly balanced with the net change being a small fraction of gains and losses. On the other hand, changes to trees, shrub and, managed grass are unbalanced; the net change is a significant fraction of gains and losses.

4. Discussion and conclusions

The foundation on which our results are built is the ESA CCI-LC series of land cover maps. Thus, ultimately, our results are only as accurate as the accuracy of the CCI-LC data (ESA, 2017). We have added value to ESA maps by encapsulating them in a much smaller and more usable product rooted in the GIS framework and focused on change over the entire span of the CCI-LC series. The basic unit of our database is a 9km × 9km tile containing 900 CCI-LC pixels. However, the attributes of a tile contain an agglomeration of change information from its constituting pixels, so the only information lost by using tiles instead of pixels is the exact position of every transition within a tile. Thus, for regions $\gg 81$ km^2, the change analysis based on our database is as accurate as the analysis based on original CCI-LC maps. In addition, our database also includes tile’s overall change trajectory type and its composition of PFTs. Using the first of these added-on features we produced a global map of landscape change during the 1992–2015 period (Supplement 1). This map helps to understand geographical distribution of various types of land change across the entire landmass. Using the second added-on feature we calculated (Table 2) change in coverage of different vegetation types.

Our decision to concentrate on the part of the landmass where a significant change in landscape had occurred on the scale of 9km × 9km tracts of land has left 78% of the landmass out of the analysis (see section 2.2). However, we have demonstrated (section 3.3) that the "changed zone" accounts for ~80% of all change in vegetation types. The remaining change is distributed across the landmass in tracts of land ≪ 81 km^2 surrounded by large areas of unchanged land, so their ecological significance is small. The vegetation type that experiences the largest loss was the trees type at -559,124 km^2 globally of which -462,179 km^2 were lost in the change zone. The second largest loss was to the shrub type at -222,292 km^2/-194,939 km^2. The vegetation type that experienced the largest gain was managed grass (crop) at +686,775 km^2/+649,132 km^2. The second largest gain was by the natural grass at +122,869 km^2/+86,871 km^2. Qualitatively the same conclusion applies to losses and gains estimated on the basis of transitions between land cover categories (Fig. 3). The largest losses were to forest and shrubland, and the largest gains were to agriculture, settlement (which has no vegetation type equivalent), and grassland.

The previous work to compare to our results is scarce. Most of the previous work had concentrated on changes to the forest cover. According to our results, the total area covered by trees (Table 2) was 33,505,300 km^2 in 1992 and 32,946,300 km^2 in 2015, the net loss of 559,000 km^2. This corresponds to an average (over 23 years) loss of ~24,300 km^2 y^{-1}. Using an earlier version of CCI-LC maps, available only for three epochs, 2000, 2005, and 2010, Li et al. (2016) estimated the total area covered by trees to be 31,501,000 km^2 in 2000. They estimated the net forest loss area of 162,327 km^2 between 2000 and 2010. This corresponds to an average (over 9 years) loss of ~18,000 km^2 y^{-1}. Thus, their rate of forest net loss is in the same range as ours, its smaller value could be accounted for by the decreasing rate of deforestation in the 2000s in comparison to the rates in 1990s (Keenan et al., 2015).

Hansen et al. (2010) estimated the total forest area to be 32,688,000 km^2 in 2000 and Hansen et al. (2013) published a global map of forest cover change between 2000 and 2012 (see http://www.globalforestwatch.org for the best presentation of this map) based on change detection in high resolution (30 m) Landsat images. They estimated the net forest loss area of 1,500,000 km^2 during this period. This corresponds to an average (over 11 years) loss of ~136,300 km^2 y^{-1}. Given that the deforestation rate has been decreasing from the 1990s (Keenan et al., 2015), a difference between our 23-years average net forest loss rate and Hansen's et al. projected average net forest loss rate over the same period is about sixfold.

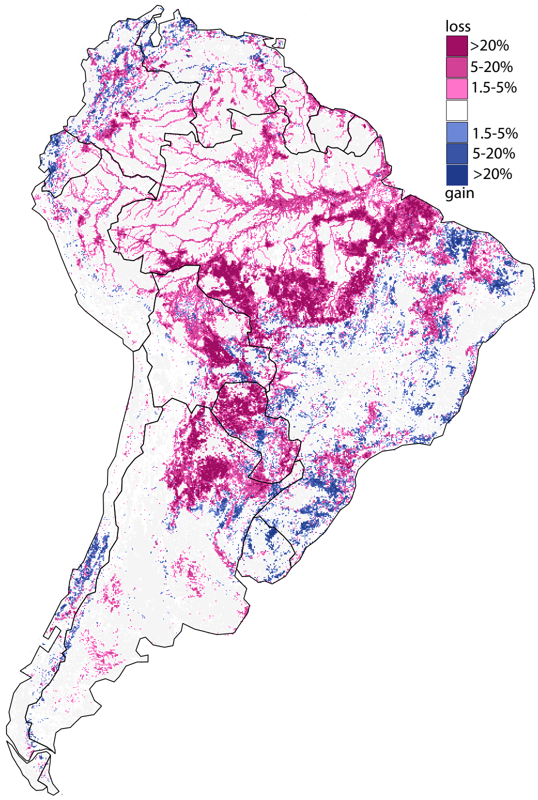

Figure 7: Map of forest losses (red) and gains (blue) in South America during the 1992-2015 period based on our calculation of tree cover. Different colors indicate the magnitude of loss/gain in units of percentage of area in a 9km × 9km tile.

Fig. 7 shows our map of forest losses/gains during the 1992-2015 period in South America. Comparison of this map to the Hansen's et al. map (http://www.globalforestwatch.org) reveals strong similarities of geographical distributions for forest losses and gains, although the gains are more widespread in our map. This conclusion extends to the global comparison of the two maps. Concurrency of loss/gain geography between the two maps is in contrast to the discrepancy between their estimates of the magnitude of forest losses/gains (see the previous paragraph). This discrepancy stems from two orders of magnitude difference in areal resolutions of the two maps, and from the CCI-LC definition of the forest category which requires as little as 15% of 300m × 300m CCI pixel's area covered by trees (ESA, 2017) to be labeled as "forest." Such definition leads to an underestimation of forest loss using a post-classification method because predominantly forested CCI-LC pixels must experience large forest loss (so their tree cover drops below 15%) before they are re-labeled to non-forest categories. In other words, statistically, losses of forest in small tracts of land are ignored by the post-classification change detection but preserved by the direct comparison of much smaller Landsat pixels. The CCI-LC definition of forest category also leads to an overestimation of forest gain, because pixels labeled as non-forest may transition to the forest category by adding tree cover to just a few percentages of their total area.

Thus, although using CCI-LC map is well-suited for a fairly accurate estimation of forest area and a depiction of a geographical distribution of forest losses/gains, it is not best-suited for accurate estimation of deforestation rate. Nevertheless, post-classification forest change detection based on CCI-LC maps provides a geographically accurate low estimate for forest losses and high estimate for forest gains. The issue described in the previous paragraph also affects other land cover categories besides forest but (we expect) to a lesser degree due to the less sensitive character of their definitions. There is no high resolution image data on, for example, changes to the area of crops, to check the validity of our expectation.

To the best of our knowledge, the analysis by Li et al. (2016) is the only previous work on transitions between land cover categories in the CCI-LC. However, they used an early version of CCI-LC maps, available only for three epochs, 2000, 2005, and 2015, and they only presented a summary of 2000–2005 and 2005–2010 transitions separately. The different spans over which the change was measured in the two studies make a direct comparison impossible. In addition, Li et al. (2016) refers to their results as "a transition matrix between PFTs". Traditionally, a transition matrix results from the count of pixels (or other equal size units of analysis) that changed their category labels. Since PFTs are not pixel category labels, the meaning of Li et al. "transitions" is unclear.

We have found that during the 1992–2015 period the top transitions were: forest → agriculture (19% of all transitions), agriculture → forest (10%), shrubland → forest (7%), and forest → shrubland (7%). Li et al. have found that during the 2000–2005 period the top transitions were forest→ crops (50%), forest → bare (17%), and forest → shrubland (14%), and in the 2005–2010 period, forest → crops (49%), crop→ forest (16%), and forest → shrub (8%). We have found that during the 1992–2015 period the top transitions to agriculture were: from the forest (60%), from shrubland (16%), and from grassland (11%). Li et al. have found that in the 2000–2005 period the top transitions to crops were from forest (82%), from shrub (8%), and from grass (6%), and in the 2005–2010 period, they were from crops (81%), from bare (11%), and from grass (5%). This may suggest that the most frequent transitions in the 1990s were somewhat different from the most frequent transitions in the 2000s.

Overall, our global spatial database of 1992–2015 landscape change provides the most easy-to-access resource for studying land cover change on the planetary scale. Unlike the original ESA maps, it is SQL-searchable and can be cross-referenced with other global databases, for example, that of terrestrial ecoregions (Olson et al., 2001). Results presented in section 3 and discussed in section 4 can be immediately reproduced from our database using GIS software. The global map of landscape change (Supplement 1) provides a visualization of the spatial distribution of all major change trajectories. It serves as a guide to a more focused use of the database. The applicability of the database to a particular problem can be inferred from our discussion (see above). Finally, additional database layers for the remaining 22 years for which CCI-LC maps are available can be calculated using a procedure described in section 2.

Acknowledgments. This work was supported by the University of Cincinnati Space Exploration Institute.

References

Barnsley, M. J., Barr, S. L., 1996. Inferring urban land use from satellite sensor images using kernel-based spatial reclassification. Photogrammetric Engineering and Remote Sensing 62 (8), 949–958.

B.Bonan, G., Levis, S., Kergoat, L., Oleson, K. W., 2002. Landscapes as patches of plant functional types: An integrating concept for climate and ecosystem models. Global Biogeochemical Cycles 16(2), 5–1–5–18.

Cai, S., Liu, D., Sulla-Menashe, D., Friedl, M. A., 2014. Enhancing MODIS land cover product with a spatialtemporal modeling algorithm. Remote Sensing of Environment 147, 243–255.

Chang, P., Krumm, J., 1999. Object recognition with color cooccurrence histograms. In: In Proceedings of IEEE Conference on Computer Vision and Pattern Recognition, Fort Collins, CO, June 23-25, 1999. IEEE Computer Society Conference.

Coppin, P., Jonckheere, I., Nackaerts, K., Muys, B., Lambin, E., 2004. Revie Article Digital change detection methods in ecosystem monitoring: A review. International Journal of Remote Sensing 25(9), 1565–1596.

DeFries, R., 2013. Why forest monitoring matters for people and the planet. In: Achard, F., Hansen, M. C. (Eds.), Global forest monitoring from Earth observation. CRC Press/ Taylor & Francis Group, pp. 1–14.

DeFries, R. S., Foley, J. A., Asner, G. P., 2004. Land-use choices: Balancing human needs and ecosystem function. Frontiers in Ecology and the Environment 2(5), 249–257.

ESA, 2017. European Space Agency Land Cover CCI Product User Guide Version 2.0. Tech. rep.

Friedl, M. A., Sulla-Menashe, D., Tan, B., Schneider, A., Ramankutty, N., Sibley, A., Huang, X., 2010. MODIS Collection 5 global land cover: algorithm refinements and characterization of new datasets. Remote Sensing Environ. 114, 168–182.

Gray, R. W., 1995. Exact transformation equations for Fuller's world map. Cartographica: The International Journal for Geographic Information and Geovisualization 32(3), 17–25.

Grimm, N. B., Faeth, S. H., Golubiewski, N. E., Redman, C. L., Wu, J., Bai, X., Briggs, J. M., 2008. Global change and the ecology of cities. Science 319(5864), 756–760.

Hansen, M. C., Potapov, P. V., Moore, R., Hancher, M., Turubanova, S., Tyukavina, A., Thau, D., Stehman, S. V., Goetz, S. J., Loveland, T. R., Kommareddy, A., Egorov, A., Chini, L., Justice, C. O., Townshend, J. R., 2013. High-resolution global maps of 21st-century forest cover change. Science 342, .850–853.

Hansen, M. C., Stehman, S. V., Potapov, P. V., 2010. Quantification of global gross forest cover loss. Proceedings of the National Academy of Sciences 107(19), 8650–8655.

Hussain, M., Chen, D., Cheng, A., Wei, H., Stanley, D., 2013. Change detection from remotely sensed images: From pixel-based to object-based approaches. ISPRS Journal of Photogrammetry and Remote Sensing 80, 91–106.

Jones, P. D., Lister, D. H., Li, Q., 2008. Urbanization effects in large-scale temperature records, with an emphasis on China. Journal of Geophysical Research: Atmospheres 113, D16122.

Keenan, R. J., A.Reams, G., Achard, F., deFreitas, J. V., Grainger, A., Lindquist, E., 2015. Dynamics of global forest area: results from the FAO Global Forest Resources Assessment. Forest Ecology and Management 352, 9–20.

Kim, D. H., o. Sexton, J., p. Noojipady, Huang, C., Anand, A., Channan, S., Feng, M., Townshend, J. R., 2014. Global, Landsat-based forest-cover change from 1990 to 2000. Remote Sensing of Environment 155, 178–193.

Li, W., Ciais, P., MacBean, N., Peng, S., Defourny, P., Bontemps, S., 2016. Major forest changes and land cover transitions based on plant functional types derived from the ESA CCI Land Cover product. International Journal of Applied Earth Observation and Geoinformation 47, 30–39.

Lin, J., 1991. Divergence measures based on the Shannon entropy. IEEE Transactions on Information Theory 37 (1), 145–151.

Lu, D., Li, G., Moran, E., 2014. Current situation and needs of change detection techniques. International Journal of Image and Data Fusion 5(1), 13–38.

Mahmood, R., Pielke, R. A., Hubbard, K. G., Niyogi, D., Dirmeyer, P. A., McAlpine, C., Carleton, A., Hale, R., Gameda, S., Beltrán-Przekurat, A., Baker, B., 2014. Land cover changes and their biogeophysical effects on climate. International Journal of Climatology 34(4), 929–953.

Netzel, P., Stepinski, T. F., 2015. Pattern-Based Assessment of Land Cover Change on Continental Scale With Application to NLCD 20012006. IEEE Transactions on Geoscience and Remote Sensing 53(4), 1773–1781.

Niesterowicz, J., Stepinski, T. F., 2016. On using landscape metrics for landscape similarity search. Ecological Indicators 64, 20–30.

Niesterowicz, J., Stepinski, T. F., Jasiewicz, J., 2016. Unsupervised regionalization of the conterminous U.S. into hierarchical landscape pattern types. International Journal of Geographical Information Science 30(7), 1450–1468.

Olson, D. M., Dinerstein, E., Wikramanayake, E. D., Burgess, N. D., Powell, G. V. N., Underwood, E. C., D'amico, J. a., Itoua, I., Strand, H. E., Morrison, J. C., Loucks, C. J., Allnutt, T. F., Ricketts, T. H., Kura, Y., Lamoreux, J. F., Wettengel, W. W., Hedao, P., Kassem, K. R., 2001. Terrestrial Ecoregions of the World: A New Map of Life on Earth. BioScience 51 (11), 933.

Poulter, B., MacBean, N., Hartley, A., Khlystova, I., Arino, O., Betts, R., Bontemps, S., Boettcher, M., Brockmann, C., Defourny, P., Hagemann, S., 2015. Plant functional type classification for earth system models: results from the European Space Agency's Land Cover Climate Change Initiative. Geoscientific Model Development 8, 2315–2328.

Poulter, B., P.Ciais, Hodson, E., Lischke, H., Maignan, F., Plummer, S., Zimmermann, N. E., 2011. Plant functional type mapping for earth system models. Geoscientific Model Development 4(4), 993–1010.

QGIS Development Team, 2017. QGIS Geographic Information System. Open Source Geospatial Foundation Project. Tech. rep., http://qgis.osgeo.org.

Radke, R. J., Andra, S., Al-Kofahi, O., Roysam, B., 2005. Image change detection algorithms: A systematic survey. IEEE Transactions on Image Processing 14(3), 294–307.

Tewkesbury, A. P., Comber, A. J., Tate, N. J., Fisher, A. L. P. F., 2015. A critical synthesis of remotely sensed optical image change detection techniques. Remote Sensing of Environment 160, 1–14.

Vitousek, P. M., Mooney, H. A., Lubchenco, J., Melillo, J. M., 1997. Human domination of Earth's ecosystems. Science 277(5325), 494–499.

Wang, J., Zhao, Y., Li, C., Yu, L., Liu, D., P. Gong, P., 2015. Mapping global land cover in 2001 and 2010 with spatial-temporal consistency at 250m resolution. ISPRS Journal of Photogrammetry and Remote Sensing 103, 38–47.

Warner, T. A., Almutairi, A., Lee, J. Y., 2009. Remote sensing of land cover change. In: Warner, T. A., Nellis, D. M., Foody, G. M. (Eds.), The SAGE Handbook of Remote Sensing. SAGE Publications, pp. 459–472.

Supplement 1